CORE
Metadata, citation and similar papers at core.ac.uk
Provided by NASA Technical Reports Server

AIRBORNE DOPPLER RADAR DETECTION OF LOW ALTITUDE WINDSHEAR

E.M. BRACALENTE, C.L. BRITT*, W.R. JONES
NASA LANGLEY RESEARCH CENTER, HAMPTON, VA.
23665

p67

N91-11689

Abstract

As part of an integrated windshear program, the Federal Aviation Administration, jointly with NASA, is sponsoring a research effort to develop airborne sensor technology for the detection of low altitude windshear during aircraft take-off and landing. One sensor being considered is microwave Doppler radar operating at X-band or above. Using a Microburst/Clutter/Radar simulation program, a preliminary feasibility study was conducted to assess the performance of Doppler radars for this application. Preliminary results from this study are presented. Analysis show, that using bin-to-bin AGC, clutter filtering, limited detection range, and suitable antenna tilt management, windshear from a "wet" microburst can be accurately detected 10 to 65 seconds (.75 to 5 Km) in front of the aircraft. Although a performance improvement can be obtained at higher frequency, the baseline X-band system simulated detected the presence of a windshear hazard for the "dry" microburst. Although this study indicates the feasibility of using an airborne Doppler radar to detect low altitude microburst windshear, further detailed studies --including future flight experiments -- will be required to completely characterize the capabilities and limitations.

Key Words

Aviation safety, windshear detection and avoidance, windshear hazard index, airborne remote sensor technology, microwave Doppler radar.

Nomenclature

A/D	Analog to Digital
AGC	Automatic Gain Control
A/C	Aircraft
c	Speed of light, m/s
CSD	Clutter Spectral Density
CSR	Clutter-to-Signal ratio
D	Rain drop diameter, mm
dB	Decibels
dBw	Decibels relative to 1 watt
dBz	Reflectivity factor in Decibels
F	Hazard factor
F_R	Radial component of hazard factor
g	Acceleration of gravity, m/s^2
G	Peak antenna gain
I&Q	In-phase and Quadrature
k	Boltzmann's constant, Joules/Kelvin
k_w	Refractive index factor for rain
l	One-way rain attenuation loss
l_r	Receiver bandwidth loss factor
ln	Natural log (to the base e)
n	Total rain reflectivity per unit volume
NRCS	Normalized Radar Cross Section
P_n	System noise power, watts
P_s	Reflected signal power, watts
P_t	Peak transmitter power, watts
PRF	Pulse Repetition Frequency
R_g	Range bin distance from A/C, m
R_T	Range to target, meters
SAR	Synthetic Aperture Radar
SCR	Signal-to-Clutter ratio
SNR	Signal-to-noise ratio
T_s	System Noise Temperature, deg. Kelvin
Tilt	Antenna angle measured from A/C glide-slope
V	Aircraft airspeed, m/s
V_c	Cell volume of rain target, m^3
W_h	Vertical component of inertial wind, m/s
W_x	Horizontal component of inertial wind, m/s
Z_e	Reflectivity factor, mm^6/m^3
τ	Transmitter pulse duration, sec.
ϕ	Antenna 3 dB beamwidth, radians
λ	Wavelength, meters

I. Introduction

Low altitude microburst windshear is recognized as a major hazard during takeoff and landing of aircraft. Microbursts are relatively small, intense downdrafts which spread out in all directions upon striking the ground. When such windshear is encountered at low altitudes during landing or takeoff, the pilot has little time to react correctly to maintain safe flight (Fig. 1). In the United States during the period 1964 to 1985, there were 26 major civil transport aircraft accidents and four incidents involving 626 fatalities and over 200 injuries for which windshear was a direct cause or a contributing factor. As part of its integrated windshear program, the Federal Aviation Administration (FAA) jointly with NASA, is sponsoring a research effort to develop airborne sensor technology for detection of low altitude windshear during A/C takeoff or landing. A primary requirement for an airborne forward-looking sensor or system of sensors is to be capable of detecting both heavy ("wet") and light ("dry") precipitation microbursts. One sensor being considered for this application is microwave Doppler radar operating at X-band or higher frequency. Since absolutely clear air produces no radar return at microwave frequencies except very slight scattering from gradients in the index of refraction on the scale of the r.f. wavelength, the emphasis in the present research is on those microburst containing at least some liquid water.

*Affiliation: Research Triangle Inst., Hampton, VA

This paper is declared a work of the U. S. Government and is not subject to copyright protection in the United States

PRECEDING PAGE BLANK NOT FILMED

Previous experiments[1] and studies have demonstrated, in a limited way, the capability of airborne Doppler radars to detect the presence of windshear. However, for A/C landing and take-off applications, the problems of severe ground clutter, rain attenuation, and low reflectivity levels must be solved. To consider these problems, a Microburst/Clutter/Radar simulation program has been developed to aid in the evaluation and development of Doppler radar concepts. The simulation program incorporates windfield and reflectivity databases derived from a high resolution numerical windshear model[2], clutter maps derived from airborne Synthetic Aperture Radar (SAR) backscatter data, and various airborne Doppler radar configurations and signal processing concepts. The program simulates the operation of a Doppler radar located in an A/C approaching a runway, sensing signal returns from a windshear microburst and an airport clutter environment. A description of the Microburst/Clutter/Radar simulation program is presented along with examples of simulation outputs.

Using this program, a preliminary tradeoff and assessment study was conducted to evaluate the performance of Doppler radars to detect windshear during A/C landing. Case study results for a straw-man design are presented, illustrating airborne Doppler radar capabilities. Results for both a "wet" and "dry" microburst are included. This preliminary study shows the feasibility of using airborne Doppler radars to detect windshear; however, further detailed studies will be required, including future flight experiments, to completely characterize their capabilities and limitations.

II. Doppler Radar Design Requirements and Performance Tradeoffs

Preliminary Design Requirements

A preliminary set of performance requirements[3] has been established for design of forward-looking windshear detection sensors. The sensors' primary requirement is to detect severe microburst windshear during final approach to landing (Fig. 1) or during takeoff, and to provide as a minimum, 15 to 40 seconds (approximately 1 to 3 km) warning to the pilot. Advisory information on windshear conditions 50 to 100 seconds (4 to 8 km) in front of the A/C is also desired. The sensor or sensor system must be able to detect windshear caused by both heavy and light precipitation microbursts. The sensor must measure mean horizontal wind speeds every 150 to 300 meters out to a range of 6 to 8 km along the flight path and a small sector (approx. 20 deg.) on either side of the A/C, with approximately 1 m/s accuracy. These primary requirements have been established as minimum guidelines for developing sensor design requirements and evaluating potential concepts. The requirements to provide other information and capabilities, such as vertical wind speeds, rain reflectivity, wind turbulence, microburst signature recognition, and various display capabilities have not been established. Guidelines for these requirements are being developed.

A major area of radar design that requires extensive development is the radar signal processing technique, which will suppress clutter interference and provide maximum windshear detection accuracy. Before these techniques can be developed and evaluated, radar parameters must be chosen and evaluated. The radar parameters chosen by the radar designer are those which go in the radar equation to compute Signal-to-Noise Ratio (SNR) performance. The SNR for a signal reflected from a distant rain cell target is approximated by the following equations:[4]

$$SNR = \frac{P_s}{P_n} = \frac{P_t\, G^2\, l^2\, l_r\, \lambda^2\, n\, V_c\, \tau}{2\ln(2)(4\pi)^3\, k\, T_s\, R_T^4} \qquad (1)$$

where:

$$P_n = k\, T_s/\tau \qquad (2)$$

$$n = 10^{-18}\, (\pi^5/\lambda^4)\, \left|k_w\right|^2\, Z_e \qquad (3)$$

$$Z_e = (1/\Delta V_c)\Sigma_j D_j^6 \qquad (4)$$

$$V_c = (\pi/4)\, R_T^2\, \phi^2 (c\,\tau/2) \qquad (5)$$

As seen from these equations a large number of parameters affect the performance of the radar. The designer, however, has control over only a few of them, mainly transmitter power, antenna gain, frequency of operation, pulse duration, and to a minor degree, target range. There is, for airborne operation, a number of factors which limits the choice of values for these parameters. The use of higher operating frequencies provides greater sensitivity to rain reflectivity[3] and higher resolution[5], but is subject to greater attenuation by rain. Most operational Doppler weather radars operate at frequencies of S-band (1-3 GHz), C-band (3-8 GHz), and X-band (8-12 GHz.). Although negligible attenuation occurs at S-band, the increase in sensitivity and smaller cell resolution at X-band outweighs the small increase in attenuation (2-5dB) experienced for "wet" microbursts. For "dry" microbursts, frequencies in the Ku-band (12-18 Ghz) region could be considered since attenuation would remain low. Windshear detection capability for both "wet" and "dry" microbursts could utilize dual frequency operation, but practical considerations make it desirable to find one frequency that can provide acceptable performance for all microbursts.

Airborne weather radars, operate in an allocated frequency band around 9.3 GHz and utilize solid state transmitters of about 100 watts. They are presently in use to display rain reflectivity and wind turbulence advisory information to the pilot. Therefore, it is of interest to assess airborne Doppler radar concepts for windshear detection operating in this frequency band utilizing relatively low powers. Space limitation in the nose radome of passenger A/C limit the maximum antenna size to about 30-36 inches (.76-.91 m) in larger A/C and about 18-20 inch in smaller A/C. This makes it more important, from a resolution and sensitivity standpoint, to operate at the higher frequencies. It is desirable to keep transmitter power requirements low so that solid state transmitters can be considered. Other radar parameters such as pulse repetition frequency (PRF), and pulse width are chosen to minimize velocity and range foldover problems and to provide acceptable range resolution. Table 1 lists the range of radar parameter values being considered in the feasibility study, and which represent state-of-the-art airborne Doppler radar hardware implementation capability. Also listed is a baseline set of values used in the initial radar simulation case studies.

Table 1 Wind shear Doppler radar parameter values

Parameter	Baseline Value	Tradeoff Range
Pulse repitition freq. (PRF)	3030	2000-5500
Pulse width (TAU) u-sec.	1.0	1.0 -3.0
Max. det. range, km	10	5 TO 10
Range gate resolution, m	150	150 TO 450
Range sampling window, km	1-9	1-10
Max. unambiguous ws, m/sec.	24	24 TO 45
Wind speed accuracy, m/sec.	1.0	.5 TO 2
Operating frequency, GHz	9.3	9.3 - 15
Antenna diameter, m	.76	.46-.91
Antenna gain, dB	35.5	31 TO 48
Antenna beamwidth, deg.	3	.8 TO 5
Sidelobe level, dB	< -25	-20 TO -35
Antenna polarization	LINEAR H	DUAL POL
Ant. tilt angle range, deg.	0 to 2	0 to 20
Azimuth angle range, deg.	+OR- 21	+OR- 45
Minimum det. signal, dBZ	0	-15 TO 10
Transmitter peak power, kw	2	.2 to 10
System noise figure, dB	4	3 TO 6
Return sig. dynam. range ,dB	70	60 - 80
Receiver dynamic range, dB	50	45 TO 55
Xmit/rec. phase jitter,d.rms	.5	.1 TO 2
Number of A/D conv. bits	12	10 TO 14
Clutter filter type	2 pole	TBD
Processing technique	PP	FFT, PP

SNR Performance

Using selected values of parameters found in table 1, a set of SNR performance curves were computed using (1). Sample plots of these SNR curves are shown in figures 2 & 3. The SNR is computed in a bandwidth equal to $1/\tau$. A SNR in this bandwidth of greater than unity (0 dB) is generally required to obtain adequate Doppler processing performance. These curves show that SNR performance exceeding 0 dB can be obtained for relatively low reflectivity levels (0 to 10 dBz) for ranges out to 10 km. Reflectivity values range from 60 dBz in the core of "wet" microbursts, to 10 to 40 dBz in the outflow region. The performance curves for both the 9.3 GHz (fig. 2) and 15 GHz (fig. 3) show more than sufficient SNR performance for these ranges of reflectivities. For "dry" microbursts the core reflectivity can be in the range of 20 to 30 dBz range, falling to -20 to +5 dBz in the outflow region. The 9.3 and 15 GHz performance for a -10 dBz reflectivity falls below 0 dB SNR at about 3 km and 6 km respectively, which are still acceptable ranges for this application. An increase in transmitter power would be required to operate down to the -20 dBz level.

Clutter Performance

The X and Ku-band SNR performance was shown in the previous section to be more than sufficient to allow adequate Doppler processing. However, one of the major problems associated with the sensing of microburst using an airborne Doppler radar is the presence of ground clutter. To assess the magnitude of this problem, an analysis of clutter spectra and clutter-to-signal (CSR) ratios was conducted, using ground clutter maps derived from well-calibrated SAR Normalized Radar Cross Section (NRCS) data as described in section III. A set of clutter maps has been produced for a number of different airports from existing sets of SAR data. Figures 4 & 5 show sample clutter-to-signal (CSR) ratio results, assuming a 10 dBz rain reflectivity signal level, for a few sample radar configurations approaching Willow Run airport. Plots are shown for a 5 km A/C range from touchdown, antenna tilt angles of 0^{o} and 2^{o} (antenna angle measured up from the A/C glide-slope of -3^{o}), and antenna azimuth angles of 0^{o} and 10^{o}. Table 2 lists the radar parameters used in these analyses. Figure 6 shows a histogram plot of the range of NRCS levels which exist in the clutter map used. The NRCS levels larger than -10 dB come primarily from urban areas and high level discrete targets.

Table 2 Radar parameters used in clutter analysis

A/C range from runway	5 & 7 km
A/C ground velocity	77 m/s
A/C glide slope	3^{o}
Frequency	9.3 GHz
Antenna Dia.	.76 m (30 in.)
Antenna edge illum.	-10 dB
Rain Reflectivity	10 dBz
Pulse width	1 u-sec.
PRf	5000
Ant. tilt angle	0 & 2 deg.
Ant. azimuth angle	0 & 10 deg.

The results of this preliminary clutter analysis show that the highest clutter levels (CSR of 30-60 dB) occur where the pulse in the main beam intersects the ground, from the urban areas, and for antenna tilt angle of 0^{o}. Two significant results are shown by these analyses, which can be utilized to greatly reduce the effects of clutter. First, lower CSR values occur at short ranges in front of the A/C, at range gates where the pulse in the main beam has not touched the ground. At these ranges the clutter is coming primarily from sidelobes, which if sufficiently low will suppress the clutter signals. For a 3^{o} beamwidth antenna pointed down at a 0^{o} tilt angle and a 5 km A/C range, the -3 dB point of the main beam first touches the ground at about 3.5 km, and the first sidelobe null point at about 2.7 km (a point about 35 seconds ahead of the aircraft). For a 2^{o} tilt these points are about 6 and 4.3 km respectively. Note in figure 4 the increase in CSR at a range of 2.5 km. This point corresponds to NRCS levels of -5 to 0 dB from a residential area about 2.5 to 3 km from the runway. The clutter level would have been much higher had the main beam been viewing this area rather than the beam sidelobes.

A second fact that is very evident in the data is the significant reduction in clutter that occurs when the antenna is tilted up from 0^{o} to 2^{o}. Thus, by limiting the range of data processing and employing proper antenna tilt control, CSR levels can be kept below 40 dB (well within the dynamic range capabilities of present day Doppler radar receiver design technology). Clutter suppression techniques can then be employed to reduce clutter to acceptable levels. Figure 7 shows a sample clutter spectral density plot for the 2.5 km range gates of figure 4 (ant. Tilt=2^{o}, Az=0^{o}, A/C at 5 km). The density levels are plotted against velocity relative to the A/C's ground velocity. With the most significant clutter spectrum energy levels contained between zero and about 4 m/s, a high pass filter with maximum attenuation at zero velocity can be employed to significantly reduce the clutter levels. The CSR shown in figure 7 will be reduced by over 25 dB if the energy below 3 m/s is filtered out. Since the most severe wind velocities of interest exist at much higher speeds (5-30 m/s), this filter will have little effect on the wind speed velocity estimation. Studies are underway to evaluate filter processing techniques which can provide optimum results. Section IV presents sample case study results of windshear detection performance, using the radar simulation program.

III. RADAR SIMULATION

General Description

The radar simulation program is a comprehensive calculation of the expected output of an airborne coherent pulsed Doppler radar system viewing a low-level microburst along or near the approach path of the aircraft. Figure 8 is a block diagram showing the major features of the simulation. Inputs to the program include the radar system parameters and large data files that contain the characteristics of the ground clutter and the microburst. The ground clutter data file consists of high-resolution (20m) calibrated Synthetic Aperture Radar (SAR) data of selected airport areas. The microburst data files provide reflectivity factors, x,y,z wind velocity components, and other meteorological parameters with a resolution of 40 meters. This database is generated by a numerical convective cloud model[2] driven by experimentally-determined initial conditions, and represents selected time periods of the microburst development.

For each range bin, the simulation calculates the received signal amplitude level by integrating the product of the antenna gain pattern and scattering source amplitude and phase over a spherical-shell volume segment defined by the pulse width, radar range and ground plane intersection. The amplitude of the return from each incremental scatterer in the volume segment is proportional to either the square root of the normalized cross-section of the ground clutter (from the clutter map) or the square root of the reflectivity factor of the water droplets in the microburst (from the microburst data base). The phase of each incremental scatterer is the sum of a uniformly distributed ($0 - 2\pi$) random phase term, a phase term due to relative aircraft-scatterer radial velocity, and normally-distributed random phase terms representing transmitter/receiver phase jitter and ground clutter random motion. The random phase terms simulating phase jitter and ground clutter motion are updated for each transmitted pulse, while the uniformly-distributed phase terms are updated for each sequence of pulses in a range bin. The phase terms representing aircraft-scatterer relative motion are linear functions of time.

Path attenuation for each incremental scatterer is determined by integrating the path losses over the transmission path. Empirical formulas[4] are used to determine the incremental path losses from the liquid water content of the microburst. Aircraft ground velocity is assumed to be known accurately so that derived Doppler frequencies can be referenced to a value of zero corresponding to that velocity.

Antenna patterns simulated include a generic parabolic antenna with size and aperture illumination taper specified by input data, and a flat-plate array antenna with a pattern similar to that found in the current generation of X-band airborne weather radars.

In the simulation, a sequence of N pulses of in-phase (I) and quadrature (Q) signal amplitudes are calculated for each range bin as discussed above and subjected to AGC amplification and A/D quantization. A simulated fast-acting AGC is used to adjust the gain of the system on a bin-by-bin basis to achieve a wide dynamic range and to prevent signal saturation (due to clutter) prior to and during A/D conversion. The I and Q pulse stream is then digitally filtered to suppress ground clutter near zero Doppler frequencies and processed using both conventional pulse-pair and spectral averaging algorithms to derive the average velocity and spectral width of the scatterers in the range bin. Further processing of the velocity data provides information on windshear and aircraft hazard factor.

Provision is made in the simulation to generate returns from a specified number of range bins over a specified azimuth scan so that simulated color displays of reflectivity, velocity, windshear, spectral width, etc., can be examined. Other outputs of the simulation include plots of power levels, velocity, spectral width, windshear hazard factor, and AGC levels vs. radar range. Doppler spectra of ground clutter and moisture as derived from the I and Q signals from each simulated range bin are also plotted.

Microburst Model

As mentioned above, the microburst model is a detailed numerical convective cloud and storm model that calculates the time history of the development of a microburst. The model uses a nonhydrostatic, compressible and unsteady set of governing equations which are solved on a three-dimensional staggered grid. The computation can be initiated from observed data and generates realistic wind fields that compare favorably with observed data such as that obtained in the JAWS study[5]. For the radar simulations to date, a 4x4 km lattice of 40x40 meter grid spacing increments (two-dimensional axisymmetric version) has been generated at selected time periods. Output parameters include the radar reflectivity factor (dBz), wind velocity components, temperature, equivalent potential temperature, pressure and moisture content (water vapor, ice, cloud droplets, rain, snow and hail/graupel). The model developed under NASA sponsorship is described in detail in references 2 and 5.

For the radar simulation cases discussed in this paper, a typical "wet" microburst and a typical "dry" microburst were selected and used to investigate radar performance at a particular instant of time. Figure 9 shows the reflectivity factors and velocity field of the axisymmetric "wet" microburst used in the radar simulation. The "dry" microburst is similar in form but with smaller dimensions, lower wind speeds, and much lower reflectivity levels. The "wet" microburst data are taken at 11 minutes after initiation of the microburst calculation and the "dry" microburst data are 23 minutes after initiation. The "wet" microburst resembles an axisymmetric version of the 2 August, 1985, Dallas-Ft. Worth storm[6] and the "dry" microburst is based on soundings taken on 14 July, 1982, within the JAWS network near Denver.

Clutter Model

The ground clutter model used for the present simulation cases is a high-resolution X-band SAR map of the Willow Run, Michigan, airport area provided by the Environmental Research Institute of Michigan (ERIM).

The SAR image files produced by ERIM provide calibrated NRCS data with a resolution of 20m. Figure 10 shows a high resolution (3m) SAR image of Willow Run airport from which this data was derived and the runway (9R) used in the simulation runs. In the simulations, the aircraft is positioned at a selected distance from the runway touchdown point on a three-degree glide slope.

A problem with the use of existing SAR data is associated with the variation of cross section with depression angle. These data were taken at depression angles ranging from approximately 18 to 50 degrees, whereas for the operational airborne radar simulated the depression angles of interest are approximately 1 to 20 degrees. To partially account for this difference, ERIM supplied an empirical depression-angle correction function that corrects the NRCS to the angle seen by the airborne radar. Since clutter sources from urban areas have cross sections that do not decrease significantly with depression angles in the ranges of interest, urban areas of the clutter map are excluded from this depression angle correction and the originally measured cross-section values are used in the simulation. Also, areas of the map with NRCS values equal to or greater than 5 dB are not corrected.

The corrections for depression angle are not entirely satisfactory, and cause an uncertainty in the clutter calculations of the preliminary cases discussed in this paper. Flight experiments using the ERIM SAR instrument will be flown in the summer and fall of 1988 to collect more representative airport clutter data with depression angles corresponding to those that would be seen by an airborne radar on the approach path. These data will provide better information of depression angle variation of NRCS for urban environments as well as other surfaces.

IV. SIMULATED RADAR PERFORMANCE

"Wet" Microburst

To examine the expected radar performance in specific situations, several cases have been simulated, as illustrated in figure 1, using the baseline system parameters given in table 1 and the ground clutter map from the Willow Run airport area. Figure 11 plots the SNR and SCR vs. radar range for a "wet" microburst that would be seen by the radar at a distance of 7 km from the runway touchdown point with the antenna tilted up 2 deg from the projected aircraft path. The microburst axis is located on the projected path 2 km from the touchdown point. The calculated reflectivity factor of the water droplets along a line corresponding to the projected aircraft path is also plotted in figure 11 for comparison to the simulated radar measurements. For this case, the SNR and SCR are high over the entire region of the microburst, with a minimum value of SCR (10dB) occurring at approximately 3 km from touchdown. This minimum value is due to high clutter power from an urban area at this location. The SNR exceeds 20 dB over the range, with approximately 18 dB difference between the near side and far side of the microburst due to path attenuation and geometrical factors (in this plot, the power levels are not corrected for the R_T^2 loss).

Figure 12 shows the calculation of the radial component of wind velocity derived from both pulse-pair and spectral averaging algorithms operating on 128 simulated I and Q pulses from the radar. This figure also plots, for comparison, the "true" wind speed, defined as the velocity component along the center line of the antenna beam. It should be noted that the true velocity, as defined, will always differ somewhat from the radar-measured velocity because the true velocity is measured along a line (the antenna center line), whereas the radar system measures a weighted (by reflectivity and antenna pattern) average of the velocity over a finite volume of the microburst.

A two-pole high-pass Butterworth filter was used to filter the I and Q pulses to suppress ground clutter. The 6 dB frequency response cutoff point is located at a Doppler frequency --relative to the A/C ground velocity-- corresponding to a radial component of wind velocity of 3 m/s, and the filter has two zeros at zero Doppler frequency. The effect of the clutter filter can be seen in figure 13, which is a plot of the Doppler spectrum in a range bin 4 km from the radar calculated with and without the clutter filter. For simulated velocity measurements, a processing threshold of 4 dB is used (i.e., the pulse-pair and spectral averaged velocities are set to zero if the radar received power is less than 4 dB greater than the noise threshold).

The simulated velocity measurements are within 2 m/s of the "true" velocity for velocities greater than 5 m/s and indicate clearly the potentially hazardous windshear associated with the microburst. To more closely indicate the windshear hazard to the aircraft, a measure called the F-factor or hazard index has been defined by Bowles.[3] This index is defined by the equation:

$$F = \frac{\dot{W}_x}{g} - \frac{W_h}{V} \qquad (6)$$

where $\dot{W}_x$ is the rate of change of the component of wind velocity along the aircraft path, g is the acceleration of gravity, W_h is the vertical component of wind velocity and V is the aircraft velocity. Values of F greater than 0.1 to 0.15 are considered hazardous to jet transport aircraft, considering aircraft type, configuration, and range of gross weights.[3]

Although a forward-looking radar sensor cannot directly measure the vertical wind component, the radial velocity component is measured directly. The first term in the equation for the F-factor can be derived from radar measurements of radial velocity as follows:

$$\text{Let} \quad \dot{W}_x = V \frac{\delta W_x}{\delta R_g} \qquad (7)$$

then

$$F_R = \frac{V}{g} \frac{\delta W_x}{\delta R_g} \qquad (8)$$

where:

δW_x = change in radial velocity between adjacent range bins

δR_g = distance between range bins

F_R = the radial component of the hazard index

This radial term is calculated in the simulation from the velocity measurements as shown in figure 12 by averaging velocity differences over 5 range bins, and results in outputs as shown in figure 14. The radial term of the hazard factor reaches a maximum value of 0.1 for this microburst, and both pulse-pair and spectral averaging algorithms give good measurements of the factor.

"Dry" Microburst

Simulation runs similar to those discussed above were also made with the "dry" microburst discussed previously. Figure 15 shows the hazard index derived by these runs using the baseline system parameters operating at 9.3 GHz. The figure indicates that although the windshear was detected, the velocity measurement with the baseline set of system parameters was somewhat noisy.

To improve the performance on the "dry" microburst, several system parameters can be changed. These trade-off studies have just been initiated. For example, to illustrate the radar performance at Ku-band, the dry microburst case discussed above was simulated using the same set of baseline parameters, except the operating frequency was changed to 15 GHz and the PRF was changed to 4878 pulses per second. Results for the Ku-band system with the dry microburst are shown in figures 16, 17, and 18. As may be seen, even though the SNR and SCR values are much lower than those with the wet microburst, the wind velocity was successfully measured over the hazardous part of the microburst. The hazard factor calculation clearly indicates the windshear hazard associated with this microburst.

Simulated Displays

The radar simulation program provides for an azimuth scan mode and the generation of simulated displays of several variables of interest. Figure 19 shows a black and white copy of a simulated (color) display of radial wind velocity for the "wet" microburst with the baseline set of radar parameters. Figure 20 is a simulated plot of the radial term of the F-factor and clearly indicates that a potential windshear hazard lies on the aircraft path. These displays should not be interpreted as recommended displays for the aircrew, since the specific method of alerting the crew to a hazard requires extensive study, which is presently under way, and will most likely consist of a warning light or alarm which may be supplemented by displays of additional information to aid the aircrew's decision-making process.

Future Simulation Development

The simulation program will be improved in the near future by incorporating more sophisticated signal processing techniques, models to represent moving ground clutter, and techniques for estimating true, nuisance, and missed hazard alarms. Considerable effort is planned to incorporate and investigate a full range of microburst/clutter environments, provide improved displays of simulation output data for evaluating performance, and to conduct extensive tradeoff and optimization studies.

V. Concluding Remarks

A preliminary tradeoff and assessment study was conducted to evaluate the performance of airborne Doppler radar sensors to detect hazardous microburst windshear during A/C landing. Using a preliminary set of performance requirements for the design of forward-looking sensors, a baseline set of radar parameters was developed for use in assessing windshear detection performance using a radar simulation program. A description was given of the simulation program, which includes excellent models of microburst wind fields, realistic clutter maps of airports, and accurate models of Doppler radar operation and signal processing.

For the baseline Doppler radar sensor configurations modeled, preliminary analyses of the computer simulation case studies show that windshear can be accurately detected 10 to 65 seconds in front of the aircraft approaching a hazardous microburst positioned in the flight path of landing aircraft. This was accomplished using a bin-to-bin AGC, clutter filtering, limited detection range, and suitable tilt management. The sensor is highly effective for the "wet" microburst where very high SNR and SCR are obtainable due to large reflectivity levels. For the "dry" microburst, with low reflectivity levels, windshear was detected, however, more tradeoff analyses and signal processing studies are needed before the performance for the "dry" microburst case can be fully assessed.

Initial simulations were conducted with a specific airport, selected microburst time instants, and the baseline radar parameters. These simulations clearly show that in realistic situations, downward-looking airborne radar sensors have the potential to detect windshear and provide information to the aircrew that will permit escape or avoidance of hazardous shear situations. Plans are underway to investigate a full range of microburst/clutter environments, conduct extensive tradeoff and optimization studies, and investigate various signal processing and clutter filtering concepts which can provide reliable windshear detection capability.

The initial simulation studies were confined to the landing approach, since it presents the most severe signal-to-clutter situation. Studies of the takeoff case are planned. Since the antenna can be tilted up, therefore providing high signal-to-clutter ratios, acceptable detection performance is anticipated for this case.

Although hazardous windshear can be detected by Doppler radar, the pilot must be alerted in a timely manner to avoid the hazard. A hazard index has been developed[3] which establishes when a threat to the performance of the A/C exists. The simulation studies showed that a Doppler radar sensor can detect the horizontal component of this index with sufficient accuracy to indicate in a timely manner that a threat exists. Further studies using this index will be conducted for various microburst types and locations relative to the A/C to assess the missed and nuisance alarm rate. Displays of additional advisory information for the aircrew will probably be required, and are under study. Output display examples from the simulation studies represent some of the information that could be provided.

The present and future simulation studies will provide a good foundation to determine the capabilities and limitations of Doppler radar concepts for the detection of microburst windshear. Flight experiments are needed to evaluate the simulation modeling and performance estimates. A flight experiment program is planned for the 1990-91 time period. The first phase of flights will involve measuring the clutter environment from selected airports during landing approaches. These data will be used to evaluate the clutter map models derived from the SAR data. A second phase of flights will collect data from severe convective storms at altitudes above 2000 feet. These data will be combined with the clutter data to be used to evaluate the performance of various signal processing concepts. Flight tests for candidate concept evaluation and demonstration would follow.

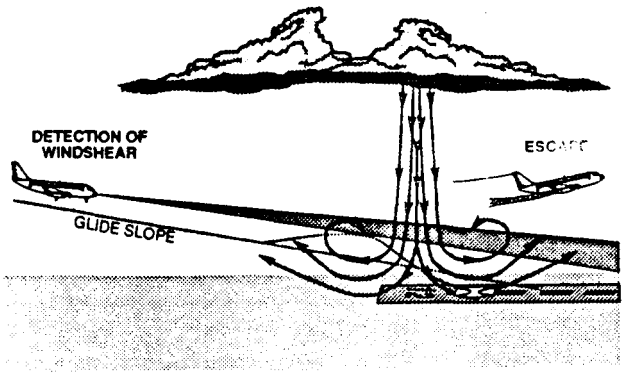

Fig. 1 Sketch illustrating the microburst windshear hazard for an approaching A/C, being probed by a radar beam. Potential impact path is shown if escape or avoidance maneuver is not activated.

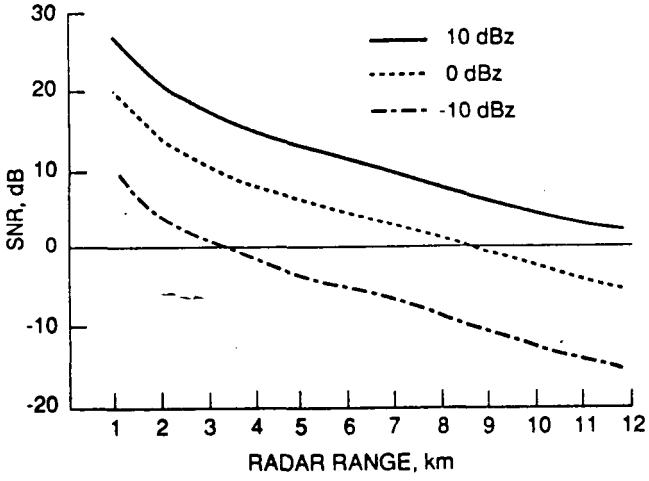

Fig. 2 Signal-to-Noise performance for different reflectivity levels, A/C 10 km from touchdown, 9.3 GHz, P_T=2 kw, τ=1 us, Ant. Dia.=30 in., Tilt=0°

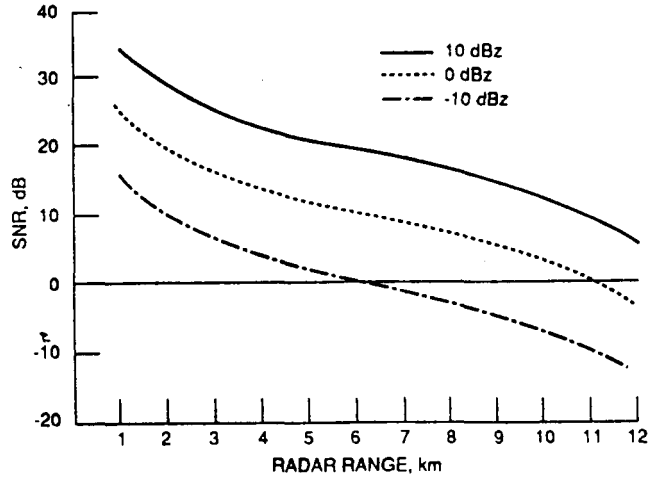

Fig. 3 Signal-to-Noise performance for for 15 GHz. All other conditions the same as in Fig. 2.

VI. References

1. Staton, L. D.: "Airborne Doppler Radar For Wind Shear Detection," In workshop proceedings, "Windshear/Turbulence Inputs to Flight Simulation & Systems Certification." NASA CP 2474, July 1987.

2. Proctor, F. H.: "The Terminal Area Simulation System Vol. I: Theoretical Formulation." NASA CR 4046: DOT/FAA/PM-86/50, I. April 1987

3. Bowles, R. L.; and Targ, R.: "Windshear Detection and Avoidance: Airborne Systems Perspective." Presented at 16th Congress of the ICAS Aug 28-Sept 2, 1988, Jerusalem, Israel.

4. Doviak, R. J.; and Zrnic, D. S.: "Doppler Radar and Weather Observations." Academic Press Inc. 1984.

5. Proctor, F. H.: "The Terminal Area Simulation System Vol. II: Verification Cases." NASA CR 4047: DOT/FAA/PM-86/50, II. April 1987

6. Bowles, R. L.; "Windshear Modeling: DFW Case Study", presented at conference "Windshear Detection Forward-Looking Sensor Technology", NASA CP 10004: DOT/FAA/PS-87/2, Oct. 1987

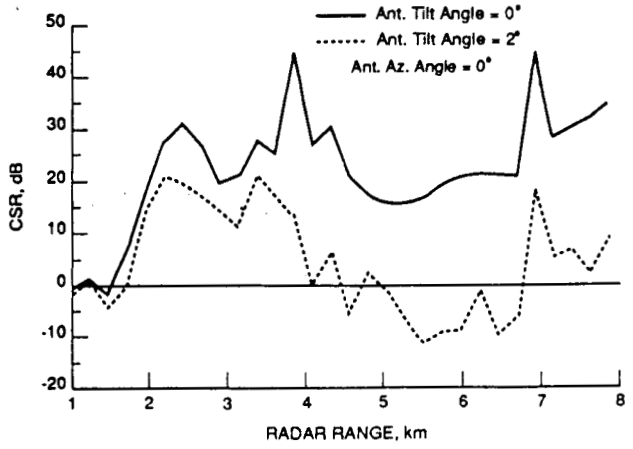

Fig. 4 Clutter-to-Signal (CSR) vs range from A/C, using Willow Run clutter map. A/C 5 km from touchdown, Ant. Az angle=0°, Z_e=10 dBz. See table 2 for other parameter values.

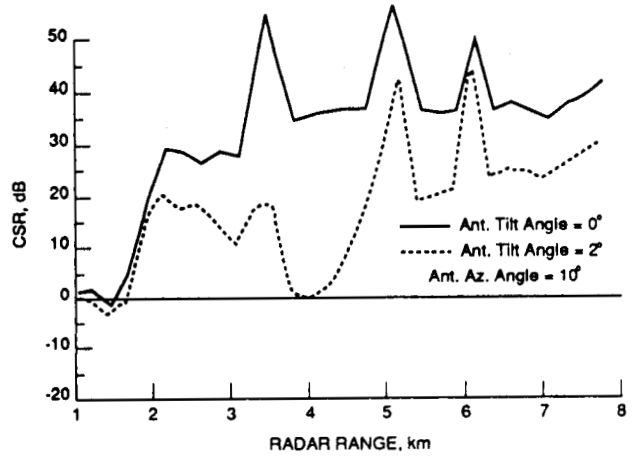

Fig. 5 Clutter-to-Signal (CSR) vs range from A/C for same conditions as fig. 4 except Ant. Az angle = 10°

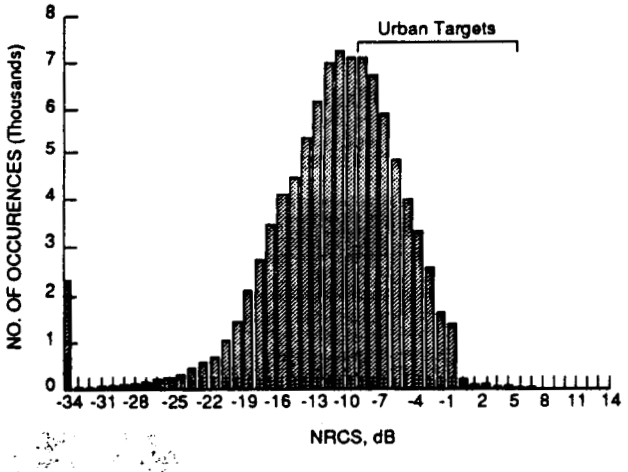

Fig. 6 Histogram plot of range of NRCS levels contained in the Willow Run Airport clutter map.

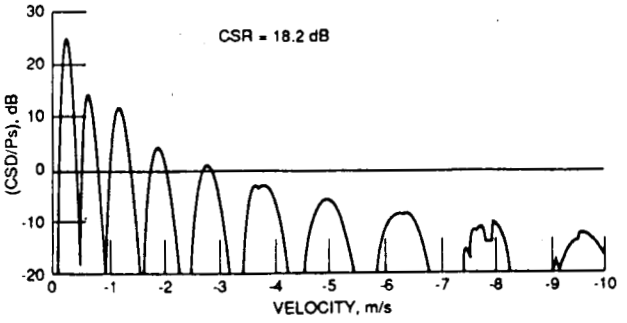

Fig. 7 Normalized clutter spectral density plot for 2.5 km range bin. A/C 5 km from touchdown, Ant. Tilt=2°, Az=0°, Z_e=10 dBz

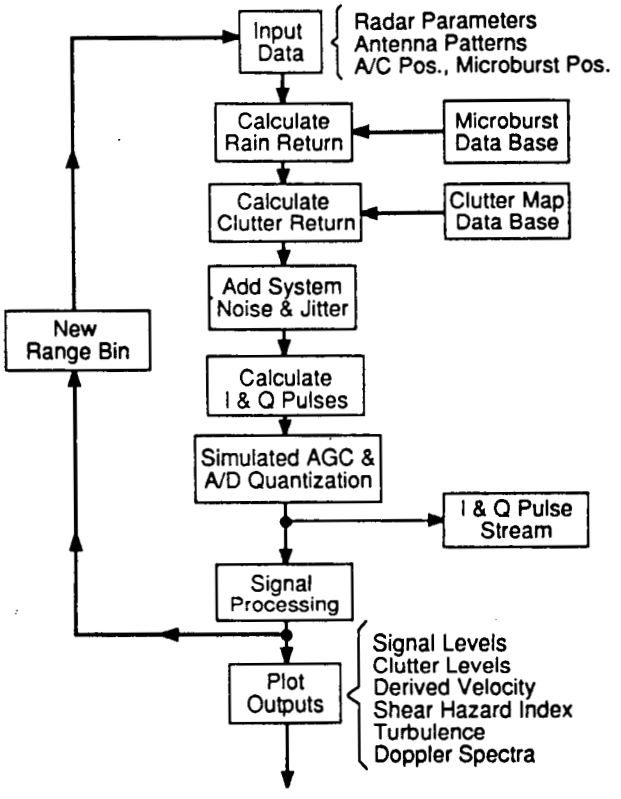

Fig. 8 Block diagram of the radar simulation program showing the major features of the simulation.

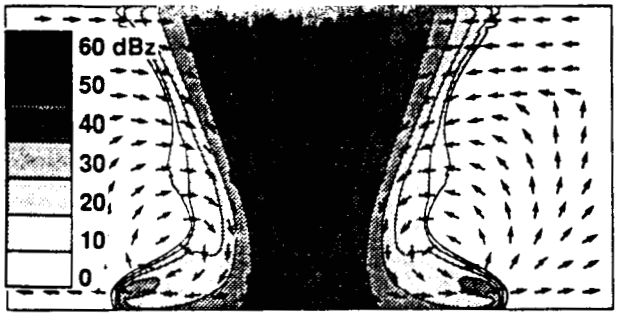

Fig. 9 Reflectivity contours and velocity field for the axisymmetric "wet" microburst model used for initial radar performance simulations studies.

Fig. 10 High resolution SAR image of the Willow Run, MI airport area. NRCS map, produced from this image data base, is used to calculate the ground clutter return in the radar simulation program.

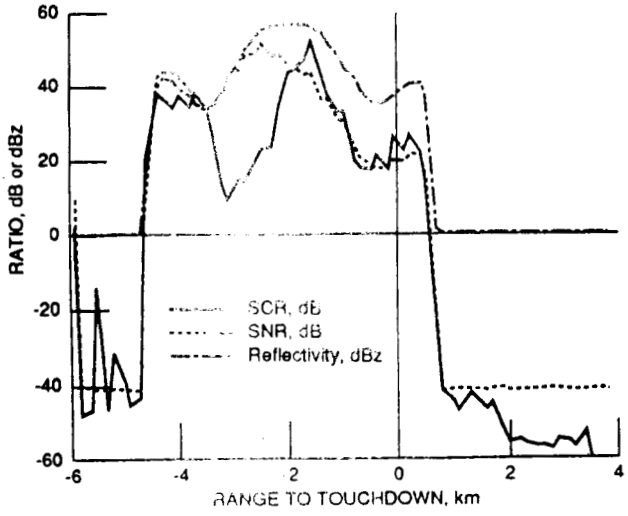

Fig. 11 Plot of calculated SNR, SCR and reflectivity factor vs range to touchdown for the "wet" microburst. Aircraft located -7km from touchdown on 3° glide slope, radar antenna tilt = 2°, microburst centered on projected flight path -2km from the touchdown point, freq.= 9.3 GHz.

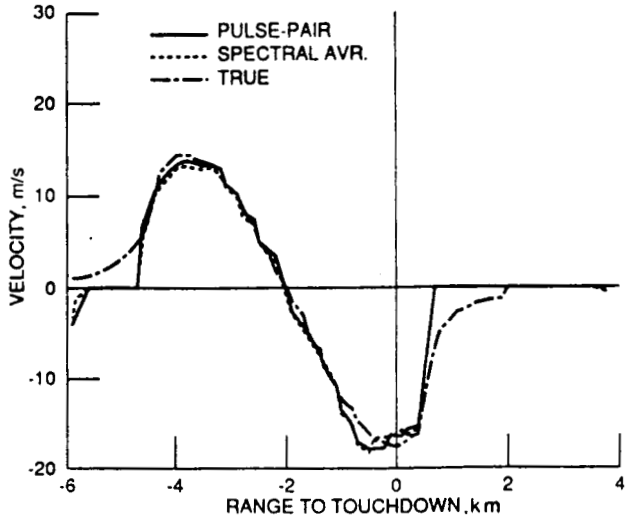

Fig. 12 Radar wind velocity measurement vs range to touchdown; same conditions as in figure 11. In this plot, positive velocities represent headwinds.

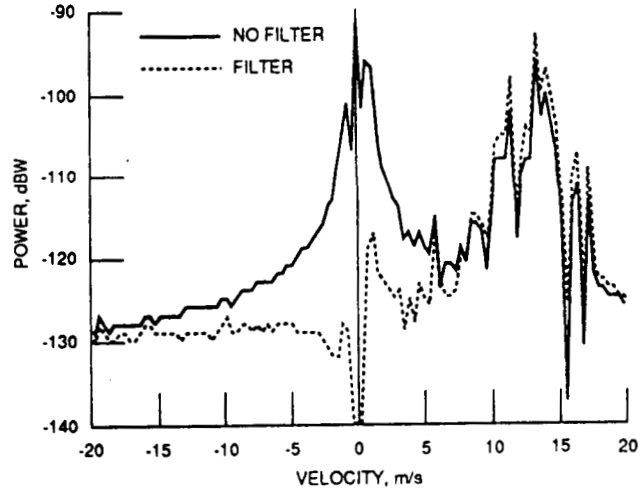

Fig. 13 Plot of Doppler spectrum from radar range bin 4km from touchdown, prior to wind velocity estimation, showing effect of 2-pole filter used to suppress ground clutter.

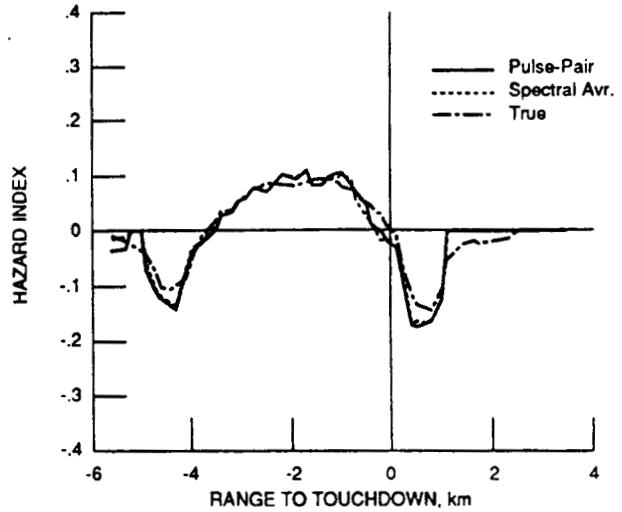

Fig. 14 Hazard index vs. range to touchdown derived from the velocities shown in figure 12. Index is calculated from average velocity differences over 5 range cells (750m).

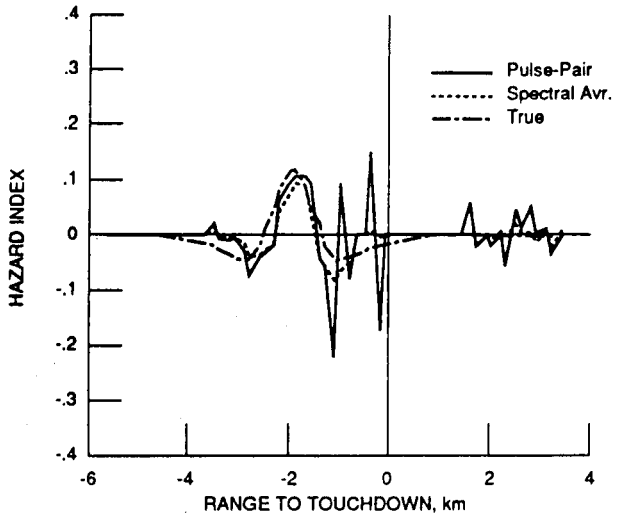

Fig. 15 Hazard index vs. range to touchdown derived from the "dry" microburst velocities using the baseline parameters, and conditions listed in fig. 11, freq. = 9.3 GHz.

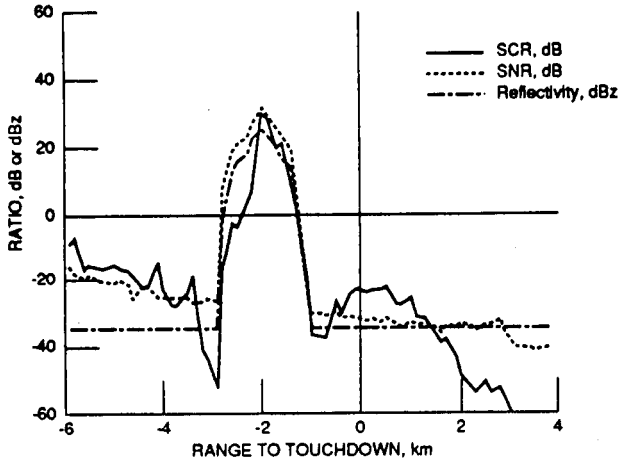

Fig. 16 Plot of calculated SNR, SCR and reflectivity factor vs range to touchdown for the "dry" microburst, and conditions listed in fig. 11, except freq. = 15 GHz.

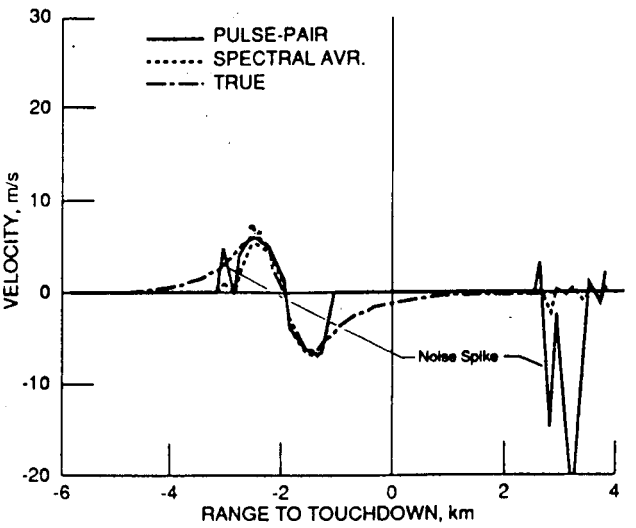

Fig. 17 Radar wind velocity measurement vs range to touchdown under same conditions as those of figure 16. The noise spikes are due to low SCR from urban clutter (-3km), and other clutter sources (+3km) where reflectivity levels are low.

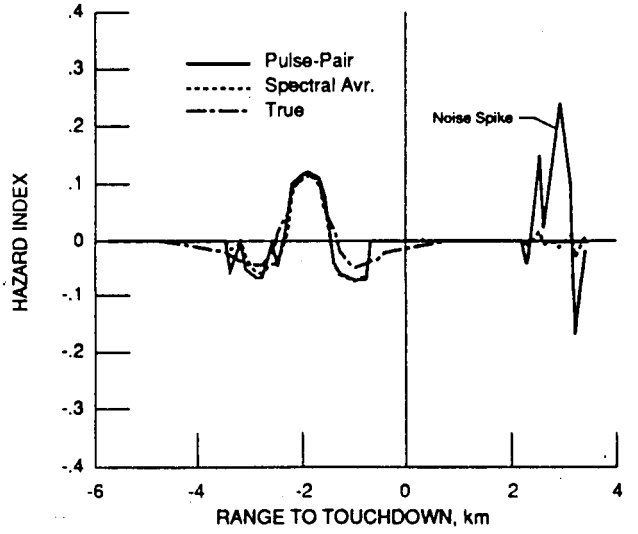

Fig. 18 Hazard index vs. range to touchdown derived from the "dry" microburst velocities shown in figure 17.

ORIGINAL PAGE IS
OF POOR QUALITY

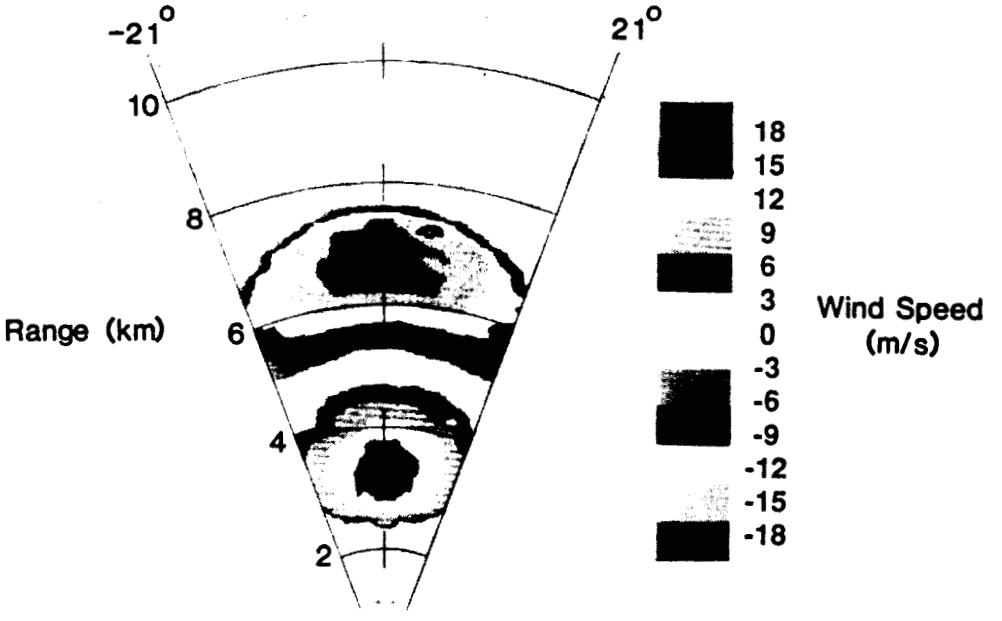

Fig. 19 Range-azimuth display of wind velocity contours for the "wet" microburst, baseline radar parameters, and conditions listed in fig. 11. The large head to tail velocity and wind direction change is clearly shown.

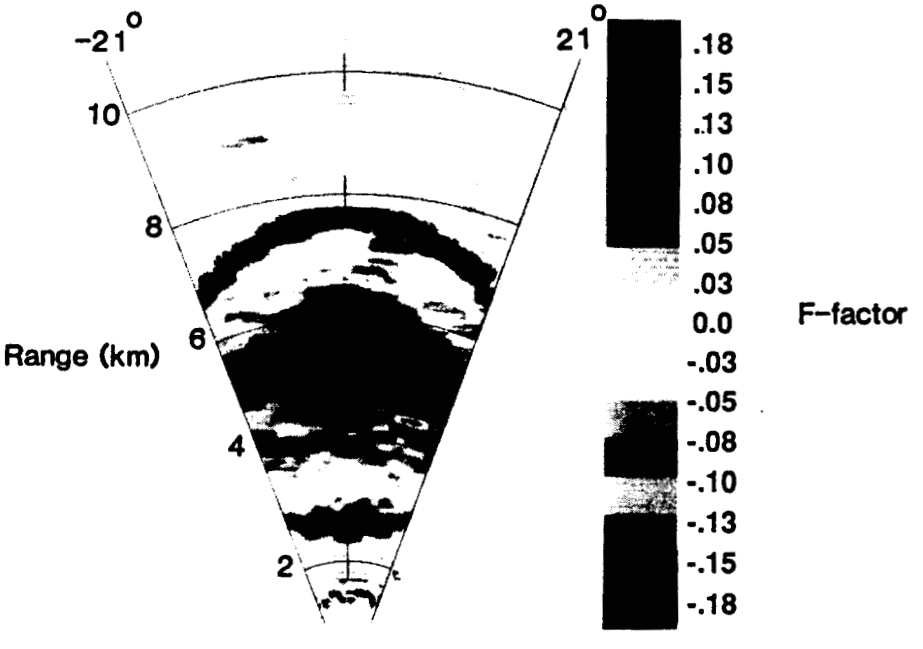

Fig. 20 Range-azimuth display of hazard index (F-factor) contours for the "wet" microburst, same conditions as fig. 19. The potential shear hazard area is clearly shown.